Nanoscale

Accepted Manuscript

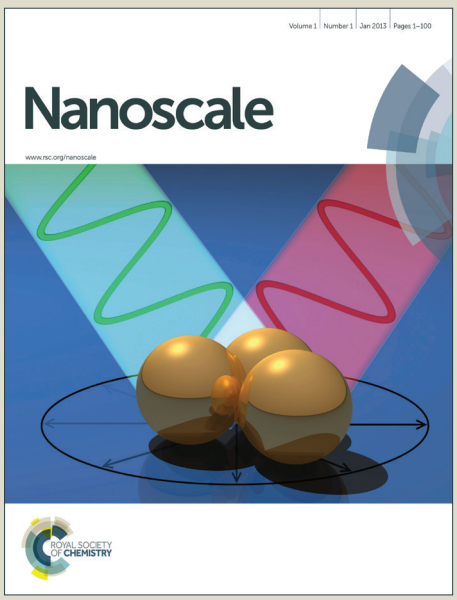

This is an *Accepted Manuscript*, which has been through the Royal Society of Chemistry peer review process and has been accepted for publication.

Accepted Manuscripts are published online shortly after acceptance, before technical editing, formatting and proof reading. Using this free service, authors can make their results available to the community, in citable form, before we publish the edited article. We will replace this *Accepted Manuscript* with the edited and formatted *Advance Article* as soon as it is available.

You can find more information about *Accepted Manuscripts* in the Information for Authors.

Please note that technical editing may introduce minor changes to the text and/or graphics, which may alter content. The journal's standard Terms & Conditions and the Ethical guidelines still apply. In no event shall the Royal Society of Chemistry be held responsible for any errors or omissions in this *Accepted Manuscript* or any consequences arising from the use of any information it contains.

ROYAL SOCIETY OF CHEMISTRY

www.rsc.org/nanoscale

Please do not adjust margins

Journal Name

COMMUNICATION

Small and light strain sensors based on graphene coated human hairs†

Received 00th January 20xx,
Accepted 00th January 20xx

DOI: 10.1039/x0xx00000x

www.rsc.org/

Wenjing Yuan, Qinqin Zhou, Yingru Li and Gaoquan Shi*

We report an efficient and cheap strategy to construct strain sensors by assembling reduced graphene oxide (rGO) sheets onto human hairs. These sensors are small, light and robust, and can be shaped into different structures such as fibre, spring and network. They can be used to detect various deformations including stretching, bending and compression with excellent repeatability and durability.

Introduction

Strain sensors can be used to detect the deformations or structural changes occurring in human bodies or in surroundings.[1–10] They are usually constructed by the composites of deformable conducting materials and flexible elastomers.[11, 12] Metallic films coated elastomeric substrates can accommodate strains by forming fractures[13] or buckling,[14] but they are limited to sensing small strains (<5%) because of their poor mechanical stabilities at high strains.[10, 11] Thus, nanomaterials have been widely explored to improve the performances of strain sensors.[12, 15, 16] Among them, graphene films have recently attracted intensive attentions, mainly due to their excellent electrical and mechanical properties. Furthermore, the unique atom-thick two-dimensional structure also makes graphene sheet easily deforms in the direction normal to its surface, providing it with good flexibility.[17–20]

On the other hand, human hair is a mechanically strong fibre with excellent flexibility. It can also be shaped into different structures by perming**.** Human hair comprises α-keratin, containing around 15–16 wt% nitrogen and 4.5–5.5 wt% sulfur;[21, 22] thus its surface have a large amount of functional groups for bonding or assembling electrically conductive components. Furthermore, a human hair has a diameter around 70 μm with very small weight. Thus, it is a promising elastic substrate for making ultrasmall and ultralight strain sensors. In this paper, we report the fabrication of strain sensors by assembling rGO sheets onto human hairs. These sensors are cheap, robust and sensitive. They are also light and small, making them comfortable with human body. Human hairs are abundant and sustainable;[23, 24] thus these strain sensors are readily scalable for practical applications.

Experimental section

Synthesis of graphene oxide (GO). GO was prepared by oxidation of natural graphite powder (325 mesh) according to the literature.[25, 26] The details are described as follows. Graphite flakes (1 g) were dispersed in concentrated sulfuric acid (24 mL), and the temperature of reaction system was kept to be around 0 ^{o}C by ice bath. Then potassium permanganate (3.0 g) was added and stirred for 16 h. Successively, diluted sulphuric acid (20 mL, 10%) was continuously added to the reaction mixture for over 2 h, then 60 mL water was added slowly for over 6 h. The reaction mixture was poured onto ice (500 mL) and hydrogen peroxide (20 mL, 3%) was added dropwisely until gas evolution was finished. The mixture was filtered and washed with 1:10 (by volume) HCl aqueous solution to remove metal ions followed by washing with water to remove the acid. The resulting cake was dried in air and diluted to form a GO aqueous dispersion (0.5% w/w). Finally, it was purified by dialysis for one or two weeks to remove the remaining impurities. The as-obtained GO dispersion was diluted to 0.35 mg mL^{-1} for use.

Perming of hair. We used our own healthy hairs cut by a pair of scissors for the experiments. These hairs were rinsed by deionized water, ethanol, and deionized water successively, and then dried in air. Then, a hair was twined onto a plastic stick (diameter = 1 mm) and immersed into the softener (Swarovski Chloe) for 30 min. After rinsing with deionized water for three times and dried, hair together with the plastic stick was immersed into the fixing lotion (Swarovski Chloe) for another 30 min. Then, rinsed with water and dried, the curled hair was released from the stick, forming a spring structure.

Self-assembly of rGO sheets. A clean straight or spring shaped hair was immersed into the aqueous solution of positively

*Department of Chemistry, Tsinghua University, Beijing 100084, People's Republic of China. E-mail: gshi@tsinghua.edu.cn. Fax: 86 62771149; Tel: 86 6277 3743.
†Electronic Supplementary Information (ESI) available: [Supplementary Figs. S1-S3]. See DOI: 10.1039/x0xx00000x

This journal is © The Royal Society of Chemistry 20xx

Please do not adjust margins

Nanoscale Accepted Manuscript

charged poly (dimethyl diallyl ammonium chloride) (PDDA, 2 wt %) for 1 h. After being washed with deionized water twice and dried in air, the modified hair was immersed into GO solution (0.35 mg mL^{-1}) for 10 min, and air dried. Then the GO/straight hair composite was soaked in hydrazine solution (60%) for 16 h to reduce its GO component. In the case of using spring-shaped sample, GO solution was adsorbed into the intervals between hair screws because of capillary force. The assembled structure was immersed into ascorbic acid solution (10 mg mL^{-1}) and kept at 70 °C for 2 h. Porous and wrinkled rGO coating was formed on the surface of hair spring after reduction. The rGO coated linear and spring-shaped hairs are nominated as rGO-l-hair and rGO-sp-hair.

Characterizations

Raman spectra were recorded on a HORIBA Jobin Yvon HR Evolution spectrometer with He–Ne 532 nm laser excitation in the range of 50–2000 cm^{-1}. Scanning electron micrographs were taken out by using a Zeiss 1540 EsB field emission scanning electron microscope (FESEM). For strain sensing tests, rGO-l-hair or rGO-sp-hair was connected to copper wires partly sealed in polydimethylsiloxane elastomer (Sylgard 184 from Dow Corning). The copper wires were connected to an electrochemical analyzer (CHI 760D potentiostat-galvanostat, CH Instruments Inc.) for measuring current responses. Repetitive and consecutive strains were applied by a Instron 3342 universal testing machine. The sensitivity of the sensor was monitored by applying a constant bias voltage of 0.5 V on the sensor and recording the conductance change upon applying a given strain.

Results and Discussion

The shapes, sizes and weights of rGO coated hairs are nearly identical to those of clean hairs because of their ultrathin graphene layers (Fig. 1a, b). Scanning electron microscope (SEM) image indicates that the hairs used by us have an average diameter of 65 μm and their surfaces have a squamose microstructure (Fig. 1c). The surface of a rGO coated straight hair shows the wrinkles of rGO sheets (Fig. 1d). The Raman spectrum of this rGO-l-hair also confirms the successful coating of rGO sheets (Fig. S1†). This spectrum displays a D-band at 1337 cm^{-1} and a G-band at 1593 cm^{-1}. The G-band is attributed to the first-order scattering of the E_{2g} mode. The D-band is associated with the structural defects related to the partially disordered structures of graphitic domains or created by the attachments of functional groups on the carbon basal plane.[27, 28] The formation of rGO coating has also be confirmed by X-ray photoelectron spectra (XPS, Fig. S2†). The C1s XPS spectrum of GO, hydrazine reduced GO on rGO-l-hair, or ascorbic acid reduced GO on rGO-sp-hair shows four types of carbon atoms: C=C (284.6 eV), C–O (286.6 eV), C=O (287.8 eV), and HO-C=O (288.9 eV).[29, 30] The peak intensity of oxygen-containing functional groups of GO was greatly decreased after chemical reduction. Actually, the C/O atomic ratio was increased from 2.38 for GO to 3.86 for hydrazine reduced GO or to 4.99 for ascorbic acid treated GO. The surface of rGO-sp-hair

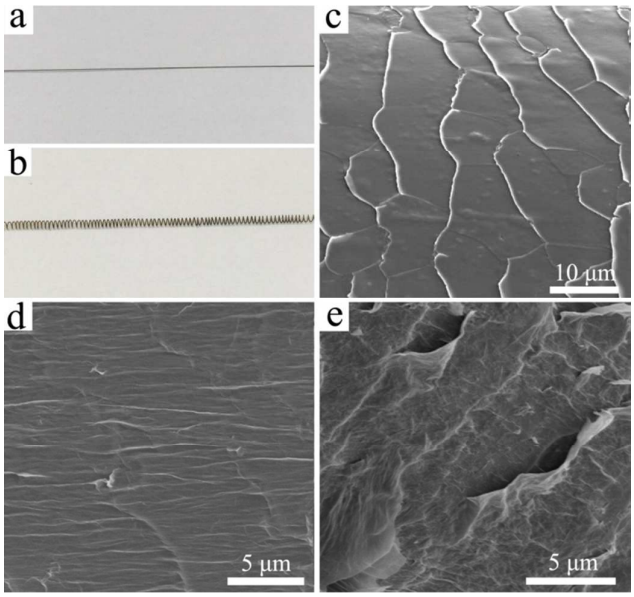

Fig. 1 (a, b) Photographs of an rGO-l-hair (a) and an rGO-sp-hair (b). (c, d) SEM images of a clean straight human hair before (c) and after (d) coating with rGO sheets. (e) SEM image of the spring-shaped hair coated with rGO sheets.

exhibits a morphology of wrinkled rGO coating with microsized cracks (Fig. 1e). This is mainly due to that the hair spring can load rGO dispersion between their neighbouring screws, forming cracks during drying because of volume contraction. An rGO coated straight hair (rGO-l-hair) can be elongated for about 30% before breaking (Fig. 2a). Upon applying a constant electrical voltage, the current flowing through rGO-l-hair decreases gradually with the increase of strain (Fig. 2b) because of the increase in its resistance. The force-strain curve has an elastic initial region with strains less than 5%. In this region, the current decreases linearly with

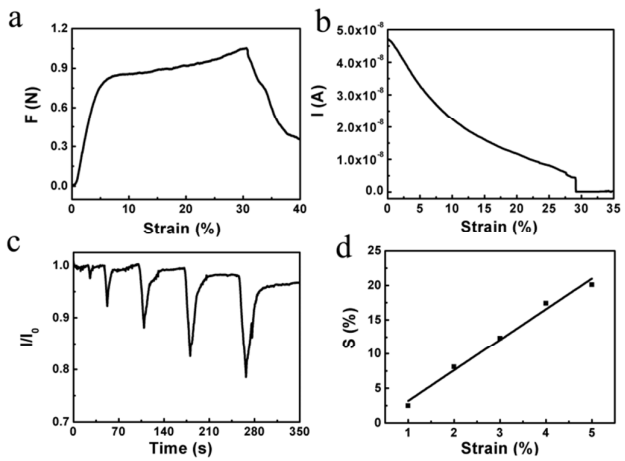

Fig. 2 (a) Force-strain curve of an rGO-l-hair composite. (b) Current-strain curve of an rGO-l-hair sensor. (c) Plot of response versus time for an rGO-l-hair sensor at a strain of 1%, 2%, 3% 4% or 5% (from left to right). (d) Plot of the response of an rGO-l-hair sensor versus strain.

Nanoscale Accepted Manuscript

This journal is © The Royal Society of Chemistry 20xx

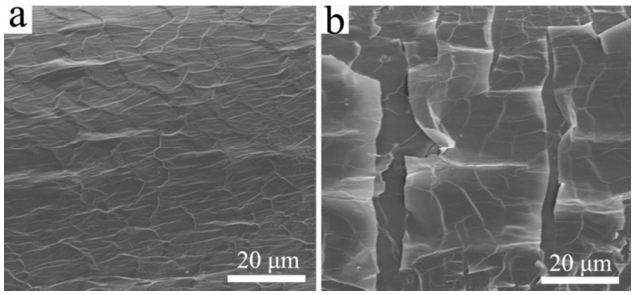

Fig. 3 (a) SEM image of an rGO-s-hair fibre in its original state. (b) SEM image of an rGO-l-hair fibre after stretching to break.

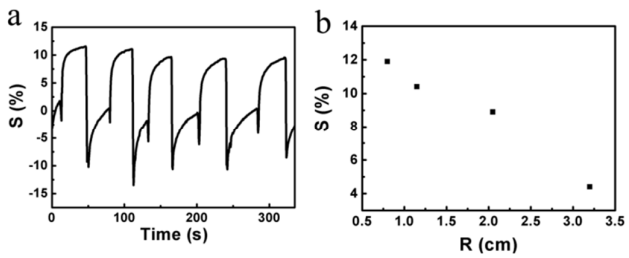

Fig. 4 (a) Current variation of an rGO-l-hair sensor upon bending to a radian of 1.15 cm for five cycles. (b) Current variation of an rGO-l-hair sensor as a function of bending radians.

strain. Therefore, the sensitivity of strain sensing (S) can be evaluated by using the equation of $S = \Delta I/I_0 \times 100\%$, where ΔI is the change in current, I_0 is the current of the sensor before stretching. It exhibits a linear relationship between $\Delta I/I_0$ and applied strain, leading to a gauge factor ($GF = (\Delta I/I_0)/\varepsilon$) of 4.46 (Fig. 2c and 2d). In order to explain the electrical response of the rGO-l-hair sensor during stretching tests, its surface morphological changes induced by stretching were examined. The surface of rGO-l-hair is uniform with rGO wrinkles in its original state (Fig. 3a). However, the rGO layer showed cracks upon stretching (Fig. 3b), making the resistance of the sensor increases with strains. At small strains, these cracks can be healed by unloading the stretching force. However, at large strains (close to the failure strain of hair), large cracks cannot be healed after unloading (Fig. 3b). It should be noted here that the sensors made from the hairs of two different persons or tested under ambient environment with different humidity showed nearly the same performances.

The performances of the strain sensors have also been applied to detect bending deformations. The rGO-l-hair sensor responded to bending deformation rapidly and the current also recovered to its original value after releasing from its bending state (Fig. 4a). More importantly, the sensing device exhibited excellent signal repeatability in each bending state. The current variation decreases with increasing bending radian, and the relative change in current at 0.8, 1.15, 2.05 and 3.2 cm bending radians were measured to be 11.9%, 10.4 %, 8.9% and 4.4%, respectively (Fig. 4b, and Fig. S3†). Accordingly, the sensing response has a linear relationship with bending radian ($S\% = -2.982R + 14.268$, where R is the bending radian). The bending of an rGO-l-hair induced additional contacts among neighbouring conductive rGO sheets at the inner side of the fibre, decreasing the contact resistances in rGO coating layer.

Human hair is a flexible substrate, its disulfur bonds can be reversibly broken and connected by redox reactions, making its shape can be remodelled. We fabricated an rGO coated hair spring (rGO-sp-hair) for compression detection. The performance of this sensor upon applying a force of 50 N for seven continuous cycles is shown in Fig. 5a. A constant current change response of 25 % was recorded. The weakest force that can be detected by this sensor was measured to be about 3 N (Fig. S4†). We performed a cycling test by repeatedly loading and unloading force. The output signals kept as a constant value upon loading, and the current returned to the baseline upon unloading the force. The relationship between relative current variation and applied force is plotted in Fig. 5b. This plot can be divided into two regions. In the low force region (3–50 N), the slope (S/F) was calculated to be 0.49 %/N. A higher force (> 50 N) caused partial saturation; thus the current response distorted from linearity. To further verify the durability of the strain sensor, a 400-cycle test was carried out by applying 10 N force. The baseline current showed a small drift (<5%) upon increasing the number of compression. This drift is mainly attributed to the thermal effect during the measurement. Nevertheless, the absolute current variation induced by the compression force was kept as a constant throughout the test (Fig. 5c), reflecting the performance of this device is repeatable. The current increase of the sensor upon compression is attributed to the enhanced contact between conductive rGO sheets. Unloading the force made the spring-shaped sensor

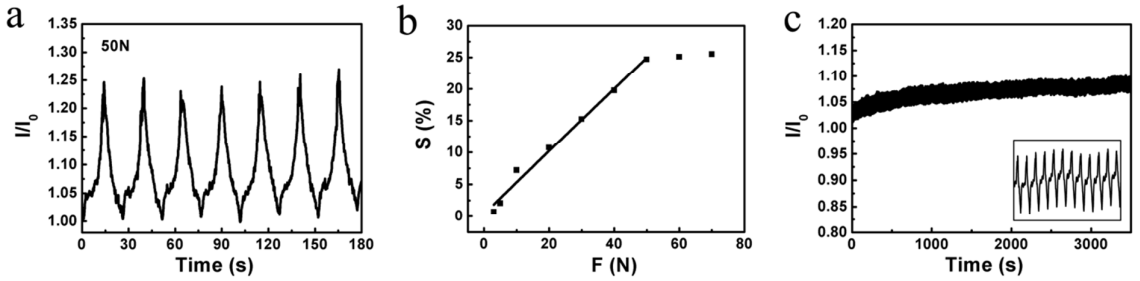

Fig. 5 (a) Current responses of an rGO-sp-hair sensor recorded during seven cycles of alternative compression and releasing. (b) Current variation of an rGO-sp-hair sensor as a function of compression force. (c) Current changes recorded during the process of compressing the sensor by a 10 N force for 400 loading/unloading cycles; the inset shows the zoomed in performance.

Nanoscale Accepted Manuscript

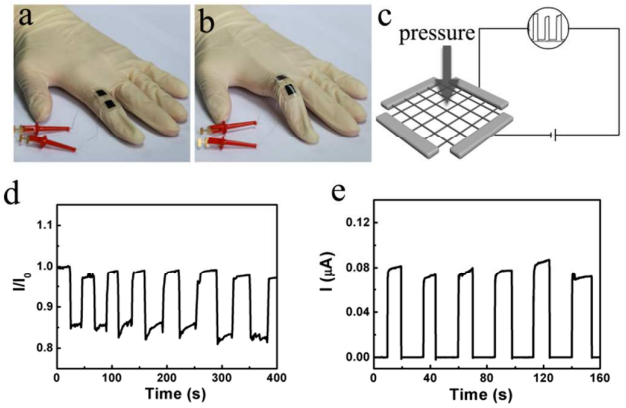

Fig. 6 (a, b) Photographs of a strain sensor fixed on an index finger in relaxing (a) and bending (b) state. (c) Schematic illustration of a 5 × 5 array network of rGO-l-hair fibres as an on-off pressure sensor. (d) The current–time response curve of an rGO-l-hair sensor that was fixed on an index finger upon different bending and releasing motions. (e) The current–time response curve of the 5 × 5 array network of rGO-l-hair fibres upon gentle finger touching.

recovered to its original shape, reducing the amount of rGO contacts and decreasing the current of the sensor at a constant applied voltage.

It is now widely accepted that environmentally benign devices is very important for future applications in daily life for health monitoring and entertainment purposes. We tested these hair-based sensors on human body to demonstrate the potential uses in wearable electronics. We mounted an rGO-l-hair sensor on the rubber glove encapsulating a finger (Fig. 6a). When bending the finger, the strain of finger was adopted by the glove layer and then, propagated to the rGO-l-hair sensor. In each bending-unbending motion, the finger bent to the same angle (about 60° as shown in Fig. 6b) in every cycle held for 20–30 s, and then released. This sensor responded to the motion of the finger rapidly and the current recovered to the original value at every bending-releasing motion. Moreover, the strain sensor performed perfectly upon repeated bending and straightening of the finger, showing good durability. The current responses were measured to be in the range of 10% to 14% (Fig. 6d). The rGO-l-hair is flexible and mechanically strong; thus it can be woven to different structures. For example, a 5 × 5 array network of rGO-l-hair was constructed and adhered onto the PDMS substrate by conductive tapes. We connected one end of the horizontal fibres and one end of the vertical fibres to conductive copper fibres (Fig. 6c). Then the network can be performed as an on-off pressure sensor. The baseline current of this network was measured to be zero. Applying a gentle finger touching on the fibre network, we can observe an immediate current increase. By repeatedly pressing down onto the strain sensor using a finger with an approximate pressure of 2 kPa, a current change from 0 to 0.08 μA was observed (Fig. 6e). This network responds to pressure rapidly and sensitively.

Conclusion

We developed prototype strain sensors based on rGO coated hairs. These sensors can detect stretching, bending and compression deformations. They have excellent mechanical stability and repeatability, while their sensitivities are moderate. The technique of fabricating sensors is convenient, cheap, eco-friendly and facile to be scaled up. A sensor is extremely small and light, like a human hair. Furthermore, human hair is an extra organismic material from self-origin. Thus, it will free from the allergic reaction if the hair is obtained from the person to whom the sensor will be implanted. Thus, this work will inspire the development of strain sensors based on human hairs for various practical applications.

Acknowledgements

This work was supported by national basic research program of China (2012CB933402, 2013CB933001) and natural science foundation of China (51433005, 21274074).

Notes and references

1 M. Segev-Bar, A. Landman, M. Nir-Shapira, G. Shuster, H. Haick, *ACS Appl. Mater. Interfaces,* 2013, **5**, 5531−5541.
2 L. Lin, Y. Xie, S. Wang, W. Wu, S. Niu, X. Wen, Z. L. Wang, *ACS Nano,* 2013, **7**, 8266−8274.
3 J. Park, Y. Lee, J. Hong, Y. Lee, M. Ha, Y. Jung, H. Lim, S. Y. Kim, H. Ko, *ACS Nano,* 2014, **8**, 12020−12029.
4 X. Xiao, L. Yuan, J. Zhong, T. Ding, Y. Liu, Z. Cai, Y. Rong, H. Han, J. Zhou, Z. L. Wang, *Adv. Mater.,* 2011, **23**, 5440−5444.
5 J. Zhao, C. He, R. Yang, Z. Shi, M. Cheng, W. Yang, G. Xie, D. Wang, D. Shi, G. Zhang, *Appl. Phys. Lett.,* 2012, **101**, 063112.
6 N. M. Sangeetha, N. Decorde, B. Viallet, G. Viau, L. Ressler, *J. Phys. Chem. C,* 2013, **117**, 1935−1940.
7 Q. Gao, H. Meguro, S. Okamoto, M. Kimura, *Langmuir,* 2012, **28**, 17593−17596.
8 D. J. Cohen, D. Mitra, K. Peterson, M. M. Maharbiz, *Nano Lett.,* 2012, **12**, 1821−1825.
9 S. Gong, W. Schwalb, Y. Wang, Y. Chen, Y. Tang, J. Si, B. Shirinzadeh, W. Cheng, *Nat. Commun.,* 2014, **5**, 3231.
10 D. Kang, P. V. Pikhitsa, Y. W. Choi, C. Lee, S. S. Shin, L. Piao, B. Park, K.-Y. Suh, T.-i. Kim, M. Choi, *Nature,* 2014, **516**, 222−226.
11 T. Yamada, Y. Hayamizu, Y. Yamamoto, Y. Yomogida, A. Izadi-Najafabadi, D. N. Futaba, K. Hata, *Nat. Nanotechnol.,* 2011, **6**, 296−301.
12 D. J. Lipomi, M. Vosgueritchian, B. C. K. Tee, S. L. Hellstrom, J. A. Lee, C. H. Fox, Z. Bao, *Nat. Nanotechnol.,* 2011, **6**, 788−792.
13 I. M. Graz, D. P. J. Cotton, S. P. Lacour, *Appl. Phys. Lett.,* 2009, **94**, 071902.
14 J. Jones, S. P. Lacour, S. Wagner, Z. Suo, *J. Vac. Sci. Technol. A,* 2004, **22**, 1723−1725.
15 K. J. Loh, J. Kim, J. P. Lynch, N. W. Shi Kam, N. A. Kotov, *Smart Mater. Struct.,* 2007, **16**, 429−438.
16 X. Li, P. Sun, L. Fan, M. Zhu, K. Wang, M. Zhong, J. Wei, D. Wu, Y. Cheng, H. Zhu, *Sci. Rep.,* 2012, **2**, 395.
17 A. K. Geim, K. S. Novoselov, *Nat. Mater.,* 2007, **6**, 183−191.
18 X. Li, R. Zhang, W. Yu, K. Wang, J. Wei, D. Wu, A. Cao, Z. Li, Y. Cheng, Q. Zheng, R. S. Ruoff, H. Zhu, *Sci. Rep.,* 2012, **2**, 870.
19 X. Huang, Z. Y. Yin, S. Wu, X. Qi, Q. He, Q. Zhang, Q. Yan, F. Boey, H. Zhang, *Small,* 2011, **7**, 1876−1902.
20 H. Tian, Y. Shu, Y. L. Cui, W. T. Mi, Y. Yang, D. Xie, T. L. Ren, *Nanoscale,* 2014, **6**, 699−705.
21 W. T. Miller, *J. Am. Chem. Soc.,* 1940, **62**, 2707−2709.

Nanoscale Accepted Manuscript

22 K. N. Chaudhari, M. Y. Song, J. S. Yu, *Small,* 2014, **10**, 2625−2636.
23 M. P. Yu, R. Li, R, Y. Tong, Y. R. Li, C. Li, J. D. Hong, G. Q. Shi, *J. Mater. Chem. A*, 2015, **3**, 9609–9615.
24 W. J. Qian, F. X. Sun, Y. H. Xu, L. H. Qiu, C. H. Liu, S. D. Wang, F. Yan, *Energy Environ. Sci.*, 2014, **7**, 379–386.
25 S. Eigler, M. Enzelberger-Heim, S. Grimm, P. Hofmann, W. Kroener, A. Geworski, C. Dotzer, M. Rockert, J. Xiao, C. Papp, O. Lytken, H. P. Steinruck, P. Muller, A. Hirsch, *Adv. Mater.,* 2013, **25**, 3583−3587.
26 J. Chen, Y. R. Li, L. Huang, C. Li, G. Q. Shi, *Carbon*, 2015, **81**, 826–834.
27 W. J. Yuan, G. Q. Shi, *J. Mater. Chem. A,* 2013, **1**, 10078–10091.
28 J. Chen, Y. R. Li, L. Huang, N. Jia, C. Li, G. Q. Shi, *Adv. Mater.*, 2015, **27**, 3654–3660.
29 J. Chen, K. X. Sheng , P. H. Luo , C. Li, G. Q. Shi, *Adv. Mater.*, 2012, **24**, 4569–4573.
30 L. Huang, Y. R. Li, Q. Q. Zhou, W. J. Yuan, G. Q. Shi, *Adv. Mater.,* 2015, **27**, 3797–3802.

Nanoscale Accepted Manuscript